OXFORD

Human Molecular Genetics, 2015, Vol. 24, No. 23 6565–6579

doi: 10.1093/hmg/ddv345
Advance Access Publication Date: 22 September 2015
Original Article

ORIGINAL ARTICLE

A role for repressive complexes and H3K9 di-methylation in PRDM5-associated brittle cornea syndrome

Louise F. Porter[1,2,4], Giorgio G. Galli[5,6], Sally Williamson[1], Julian Selley[7], David Knight[7], Nursel Elcioglu[8], Ali Aydin[9], Mustafa Elcioglu[10], Hanka Venselaar[11], Anders H. Lund[6], Richard Bonshek[2,3], Graeme C. Black[1,12,†,*] and Forbes D. Manson[1,†]

[1]Centre for Genomic Medicine, Institute of Human Development, Faculty of Medical and Human Sciences, University of Manchester, Manchester Academic Health Science Centre (MAHSC), Manchester, UK, [2]Manchester Royal Eye Hospital, Institute of Human Development, Faculty of Medical and Human Sciences, University of Manchester, Manchester Academic Health Science Centre, Manchester, UK, [3]National Ophthalmic Pathology Service Laboratory, Department of Histopathology, Central Manchester University Hospitals NHS Foundation Trust, Manchester, UK, [4]Department of Eye and Vision Science, Institute of Ageing and Chronic Disease, University of Liverpool, Liverpool, UK, [5]Stem Cell Program, Boston Children's Hospital, Harvard Stem Cell and Regenerative Biology Department and Harvard Stem Cell Institute, Harvard University, Boston, MA, USA, [6]Biotech Research and Innovation Centre and Centre for Epigenetics, University of Copenhagen, Copenhagen, Denmark, [7]Faculty of Life Sciences, Michael Smith Building, Manchester, UK, [8]Department of Pediatric Genetics, Marmara University Medical School, Istanbul, Turkey, [9]Department of Ophthalmology, University of Medipol Medical Faculty, Istanbul, Turkey, [10]Department of Ophthalmology, Okmeydani Research and Training Hospital, Istanbul, Turkey, [11]Centre of Molecular and Biomolecular Informatics, Radboudumc Institute for Molecular Life Sciences, Nijmegen, The Netherlands and [12]Centre for Genomic Medicine, Central Manchester University Hospitals NHS Foundation Trust, MAHSC, Manchester, UK

*To whom correspondence should be addressed at: Manchester Centre for Genomic Medicine, Central Manchester University Hospitals NHS Foundation Trust, Manchester M13 9WL, UK. Tel: +44 1612766094; Email: graeme.black@manchester.ac.uk

Abstract

Type 2 brittle cornea syndrome (BCS2) is an inherited connective tissue disease with a devastating ocular phenotype caused by mutations in the transcription factor PR domain containing 5 (*PRDM5*) hypothesized to exert epigenetic effects through histone and DNA methylation. Here we investigate clinical samples, including skin fibroblasts and retinal tissue from BCS2 patients, to elucidate the epigenetic role of PRDM5 and mechanisms of its dysregulation in disease. First we report abnormal retinal vascular morphology in the eyes of two cousins with BCS2 (*PRDM5* Δ exons 9–14) using immunohistochemistry, and mine data from skin fibroblast expression microarrays from patients with *PRDM5* mutations p.Arg590* and Δ exons 9–14, as well as from a PRDM5 ChIP-sequencing experiment. Gene ontology analysis of dysregulated PRDM5-target genes reveals enrichment for extracellular

[†]These authors contributed equally.

Received: June 6, 2015. **Revised:** July 29, 2015. **Accepted:** August 18, 2015

matrix (ECM) genes supporting vascular integrity and development. Q-PCR and ChIP-qPCR confirm upregulation of critical mediators of ECM stability in vascular structures (*COL13A1*, *COL15A1*, *NTN1*, *CDH5*) in patient fibroblasts. We identify H3K9 di-methylation (H3K9me2) at these PRDM5-target genes in fibroblasts, and demonstrate that the BCS2 mutation p.Arg83Cys diminishes interaction of PRDM5 with repressive complexes, including NuRD complex protein CHD4, and the repressive chromatin interactor HP1BP3, by co-immunoprecipitation combined with mass spectrometry. We observe reduced heterochromatin protein 1 binding protein 3 (HP1BP3) staining in the retinas of two cousins lacking exons 9–14 by immunohistochemistry, and dysregulated H3K9me2 in skin fibroblasts of three patients (p.Arg590*, p.Glu134* and Δ exons 9–14) by western blotting. These findings suggest that defective interaction of PRDM5 with repressive complexes, and dysregulation of H3K9me2, play a role in PRDM5-associated disease.

Introduction

Brittle cornea syndrome (BCS) is a rare, autosomal recessive, multisystemic, connective tissue disorder that is associated with extreme corneal thinning and a high risk of spontaneous corneal rupture (1,2). The condition is caused by mutations in the transcription factors zinc finger protein 469 (ZNF469) (BCS type 1 [MIM 229200]) (3) and PR domain containing 5 (PRDM5) (BCS type 2 [MIM 614161]) (4), suggested to act on a common pathway regulating extracellular matrix (ECM) proteins (4,5).

PRDM5, a member of the PR-domain family of transcription factors, is hypothesized to exert epigenetic effects through histone and DNA methylation (6) and chromatin organization (7). The PRDM5 protein has a tandem array of 16 zinc fingers and an N-terminal PR domain (related to the SET domain) that facilitates protein–protein interactions. It recognizes a consensus DNA-binding sequence supporting its direct role in transcriptional regulation (6,8–10). Many roles for the transcriptional regulator PRDM5 in gene expression have been suggested, however the mechanisms by which mutations in *PRDM5* cause disease are not understood. A role for PRDM5 as a direct activator of collagen genes has been reported (10). This role is supported by the observation of a significant downregulation of structural collagens in fibroblasts of patients with BCS2 (4). PRDM5 has, however, also been prominently associated with transcriptional repressive (6), and growth suppressive activities, including acting as a putative tumour suppressor (6,11), since reduced *PRDM5* expression has been observed in breast, cervical, gastric and lung cancers (11–16). In addition mouse Prdm5 plays a role in chromatin organization by interacting with the TFIIIC complex proteins and CTCF in embryonic stem cells (7). Both CTCF and the TFIIIC complex have been shown to have insulator functions, providing a mechanism to ensure the separation of euchromatic and heterochromatic domains, thus ensuring the stable inheritance of lineage-specific gene expression patterns.

The role of PRDM5 in epigenetic regulation is not fully understood. It is unknown whether the PR domain of PRDM5 possesses intrinsic histone methyltransferase activity, or whether it acts by recruiting the H3 lysine 9 methyltransferase EHMT2 (G9a) and interacting with histone deacetylases HDAC1 and HDAC2 (6). G9a is the predominant lysine methyltransferase of ocular tissue (17,18) preferentially producing H3K9 di-methylation (H3K9me2) (17–20), which is associated with transcriptional repression (21,22) and is a marker of inactive euchromatin (17,19,21). During retinal development, H3K9me2 has a distinctive temporal and spatial expression pattern (17). Knockdown of G9a in zebrafish (22), and its conditional knock-out (CKO) in retinal progenitor cells (18), results in decreased H3K9me2 and retinal morphological abnormalities (18,22).

In this study we investigate clinical samples from BCS2 patients with different mutations and near-identical clinical presentations. We propose a role for PRDM5 in vascular development, observing abnormal retinal vascular morphology in the eyes of two cousins with BCS2 (*PRDM5* Δ exons 9–14) using immunohistochemistry. We identify dysregulated PRDM5-target genes in skin fibroblasts from patients with two different *PRDM5* mutations (p.Arg590* and Δ exons 9–14). Our analysis highlights upregulation of a subset of PRDM5-target genes that are enriched for H3K9me2 in patient fibroblasts.

We identify a component of the NuRD co-repressor complex involved in vascular integrity during embryonic development, CHD4 (23) and the repressive chromatin interactor heterochromatin protein 1 binding protein 3 (HP1BP3), as novel PRDM5-interaction partners. These interactions were disrupted in mutant PRDM5 with a missense mutation predicted to disrupt ligand binding with S-Adenosyl Methionine and its methylation reaction product, S-adenosyl-L-homocysteine (AdoHcy). Lastly, we show that the loss of PRDM5 dysregulates H3K9me2 in BCS2 patient fibroblasts and HP1BP3 expression in retinal tissue. Together our data suggest that PRDM5-associated disease may be associated with defective interaction of PRDM5 with repressive complexes, and altered epigenetic modifications surrounding the regulation of H3K9me2.

Results

PRDM5 mutations and associated phenotypes

A summary of clinical samples used in this study is shown in Table 1.

The *PRDM5* mutation Δ9–14 is carried by cousins P1 and P2. Their clinical details have been described previously and include significant corneal thinning, corneal rupture after minor trauma, blue sclera, myopia, scoliosis and joint hypermobility (4). Δ9–14 is an in-frame deletion mutation resulting in the production of a smaller, internally deleted protein abrogating zinc fingers 6–13 that has been confirmed by western blotting.

The *PRDM5* mutation c.1768C>T p.Arg590* is carried by P3 whose clinical description includes significant corneal thinning, blue sclera, myopia and joint hypermobility (4). This mutation results in a protein truncation that has been confirmed by western blotting.

The *PRDM5* mutation c.247C>T p.Arg83Cys is carried by P4, whose clinical details are shown in Figure 1A. This mutation is within the PR-SET domain of the protein, a highly conserved region where another *PRDM5* mutation has also been described (Supplementary Material, Fig. S1 and Fig. 1B). Based on functional studies and the crystal structure of PRDM9, our computer modelling experiments suggest the arginine residue at position 83 is necessary for the binding of the ligand S-Adenosyl Methionine and its methylation reaction product, S-adenosyl-L-homocysteine (AdoHcy), formed after donation of the methyl group of S-adenosylmethionine to a methyl acceptor (24) (Supplementary Material, Fig. S2).

The *PRDM5* mutation c.400G>T p.Glu134* is carried by P5, whose clinical details include blue sclera, significant corneal thinning, high myopia with choroidal neovascularization,

Table 1. Details of the clinical samples and mutations used in the study *PRDM5* (NM_018699.2)

Clinical samples/construct	Age	Sex	Pathology	*PRDM5* mutation	Mutation consequence	Application[a]
P1 (eye and skin fibroblasts)	10	M	BCS	Δ9–14 exons	Smaller, internally deleted protein product (WB confirmation)	Histology/IHC Q-PCR/WB
P2 (eye and skin fibroblasts)	21	F	BCS	Δ9–14 exons	Smaller, internally deleted protein product (WB confirmation)	Histology/IHC Q-PCR/WB
P3 (skin fibroblasts)	8	M	BCS	c.1768C>T p.Arg590*	Truncated product (WB confirmation)	Q-PCR/WB
P4 (skin fibroblasts)	26	F	BCS	c.400G>T p.Glu134*	Presumed null	WB
P5 (expression construct)	9	F	BCS	c.247C>T p.Arg83Cys	Missense mutation	Pull-down
Control post-mortem eye #2	48	M	None	Wild-type		Histology/IHC
Control post-enucleation corneal trauma		M	Corneal trauma	Wild-type		Histology
Control skin fibroblasts (4120)	20	F	None	Wild-type		Q-PCR and WB
Control skin fibroblasts (L10)	12	M	None	Wild-type		Q-PCR and WB
Control skin fibroblasts (107)	19	F	None	Wild-type		Q-PCR
Control skin fibroblasts (#2)			None	Wild-type		ChIP-QPCR

[a]Histology: human eye; IHC: human eye; Q-PCR: skin fibroblasts; WB: skin fibroblasts; ChIP-QPCR: skin fibroblasts.

scoliosis, arachnodactyly and joint hypermobility. The mutated nucleotide is in exon 4 and this mutation is predicted to result in nonsense-mediated decay of the RNA transcript (Fig. 1B).

Retinal vascular abnormalities in BCS-type 2 eyes

Immunohistochemistry was performed on the enucleated eyes of two cousins with PRDM5-associated disease who had suffered corneal perforations spontaneously (P1) or after minor trauma (P2) (4) (Table 1). Both carried a pathogenic in-frame deletion of exons 9–14 in *PRDM5*. Both eyes had retinal thinning and reduced cell densities in the inner nuclear layer (INL) and outer nuclear layer (ONL) (Fig. 2). Extracellular matrix components were diminished around retinal capillaries with decreased capillary staining for collagens I, III and V (Fig. 2A). Other retinal microvascular abnormalities included a paucity of retinal capillaries, with reduced staining for the endothelial marker CD31 (Fig. 2A and B).

Dysregulation of ECM genes associated with vascular biology in patient fibroblasts

To identify direct targets of PRDM5 that may contribute to retinal vasculature, we were guided by expression microarray data of dermal fibroblasts from two previously reported patients with PRDM5-associated disease (P2, *PRDM5* Δ9–14; and P3, *PRDM5* p.Arg590*; Table 1) (4) and results from a PRDM5 ChIP-seq experiment in MC3T3 pre-osteoblastic cells derived from mouse (C57BL-6) calvarial osteoblasts (10). Our expression microarray analysis of patient fibroblasts identified 417 overlapping transcripts with a fold change >3 in one patient cell line, and >1.5 in the second patient cell line, in the same direction of effect, relative to age and sex-matched controls (Supplementary Material, Table S1). Using the PRDM5 ChIP-sequencing data, we compared PRDM5 peaks for these 417 most differentially up and downregulated transcripts, and after removal of redundant probes, identified PRDM5 peaks with high confidence in 43 out of 178 upregulated genes (24.2%), and 83 out of 239 downregulated genes (35%) (Supplementary Material, Table S2A and B and Supplementary Material, Fig. S3). Gene ontology analysis of these 126 differentially regulated PRDM5-bound genes revealed enrichment for genes implicated in blood vessel development and maintenance (Table 2A and B). In addition, we noted that 30% of upregulated PRDM5-bound genes, and 34% of downregulated PRDM5-bound genes in patient fibroblasts were ECM components, a number of them with roles in blood vessel development and structural integrity (http://matrisomeproject.mit.edu) (Supplementary Material, Table S2A and B). Enrichment of dysregulated downregulated PRDM5-bound genes in patient skin fibroblasts was statistically significant using a hypergeometric test (Table 2C). We confirmed the downregulation of ECM-associated genes *COL4A2*, *BGN* and *PLOD2* by qPCR (Supplementary Material, Fig. S4). Confirmation of upregulated ECM-associated genes *COL13A1*, *COL15A1*, *NTN1*, *CDH5*, that play important roles in blood vessel development and maintenance of vascular integrity, was also performed by qPCR in patient fibroblasts (Fig. 3A and Supplementary Material, Table S3). PRDM5 binding to the promoters of *COL13A1*, *NTN1* and *COL15A1* was also validated by ChIP-qPCR in skin fibroblasts (Fig. 3B). Our findings suggest that PRDM5 directly targets ECM genes involved in blood vessel biology, in agreement with our observation of retinal capillary morphological abnormalities in the eyes of two patients with BCS2.

PRDM5 interacts with CHD4-containing NuRD complex proteins and HP1BP3

PRDM5 has been reported to interact with the histone lysine methyltransferase G9a, leading to transcriptional repression (6). After identifying further PRDM5-interacting partners by pull-down we then assessed whether these interactions were affected by a novel *PRDM5* BCS-type 2 mutation in patient P4 (c.247C>T p.Arg83Cys).

First, we analysed PRDM5-interacting proteins from lysates of HEK293 cells expressing myc-tagged wild-type (WT) PRDM5. Spectral counting analysis was employed to assess relative enrichment of each interaction for WT PRDM5 versus a mock transfected cell control. As PRDM5 is a transcription factor with a predominantly nuclear localization (15), only those proteins with ≥3-fold enrichment in cells expressing WT PRDM5 (versus control) and with a nuclear or unknown cellular location identified by gene ontology analysis were retained. In total 71 PRDM5-interacting proteins were identified using these criteria

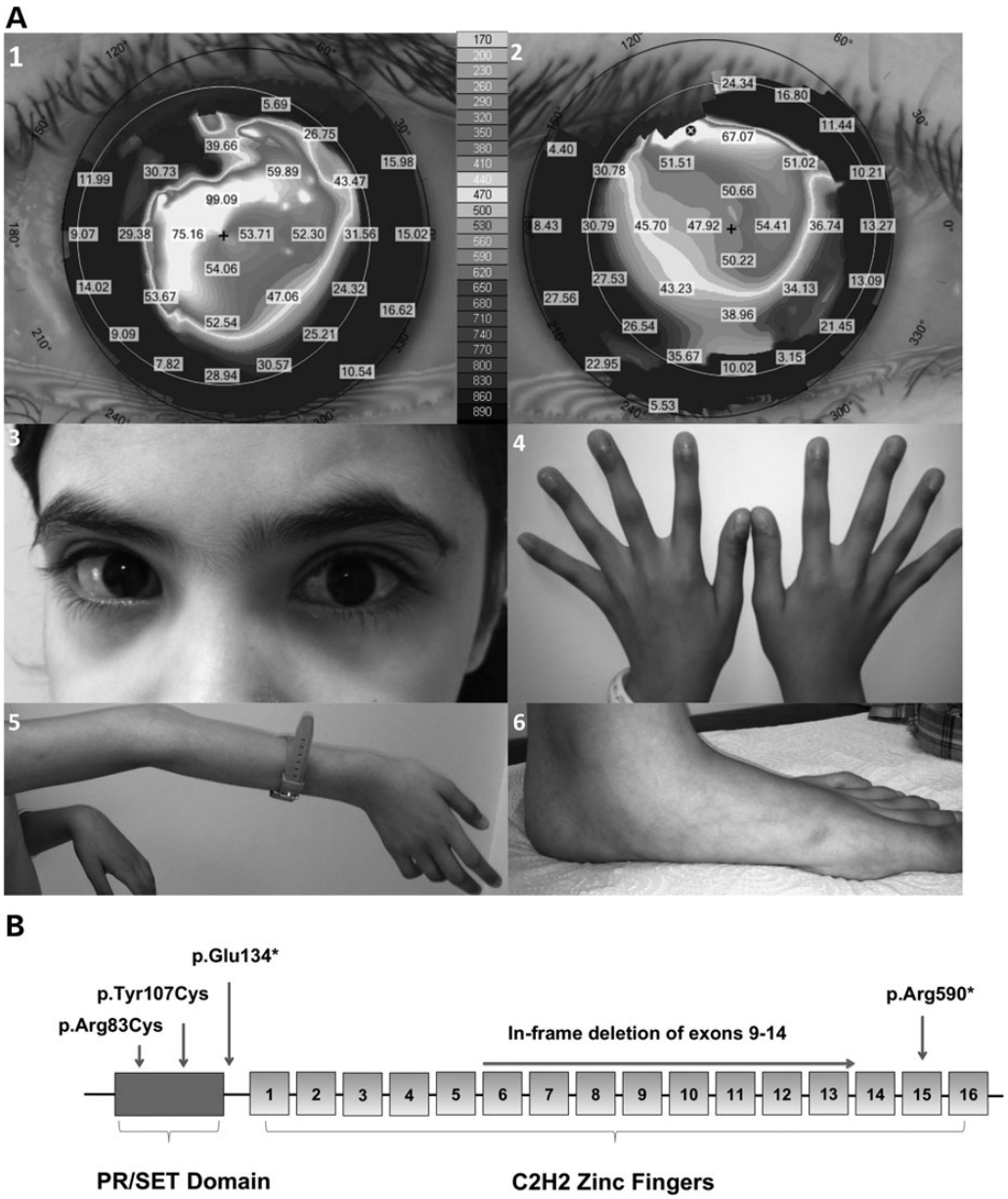

Figure 1. Clinical features of patient P4 and schematic diagram of PRDM5. (**A**) Clinical features of patient P4 (Table 1), a 9-year whose phenotype includes marked corneal thinning with central corneal thickness measurements of 350 µm left eye and 380 µm right eye (normal range 515–565 µm), shown in panels 1 and 2 (corneal topography maps). Marked irregular astigmatism is also present, shown by the K-values in the grey boxes (panels 1 and 2). (3) Photograph of the affected child reveals characteristic sclerae. Extraocular features of BCS were present in this patient and include arachnodactyly (4), joint laxity, particularly in large joints of the upper extremities (5) and pes planus (6). (**B**) Schematic diagram of PRDM5 showing the N-terminal PR-SET domain and 16 zinc fingers. Location of the novel mutation p.Arg83Cys is shown with the previously published mutations p.Tyr107Cys, mutation p.Glu134*, internal deletion of exons 9–14 and p.Arg590*.

(Supplementary Material, Table S4). Using DAVID gene ontology analysis, nuclear PRDM5-interacting proteins were classified according to biological functions. Fifteen proteins were assigned to DNA-dependent transcriptional regulation, six to RNA-polymerase II transcription and six to chromatin modification/remodelling and DNA replication and repair processes, including proteins associated with the NuRD complex. Seven proteins were associated with the regulation of mRNA translation and transport, and another 11 with nuclear splicing of mRNA (Supplementary Material, Table S5).

We identified a number of proteins involved in transcriptional repression as PRDM5-interacting partners, including NuRD co-repressor complex component CHD4, and HP1BP3 [a member of the repressive HP1 complex that binds H3K9 methylated genomic regions (25)] (Table 3). The interaction between PRDM5 and several NuRD complex components and HP1BP3 was validated by co-immunoprecipitation using a HA-tagged PRDM5 construct (Fig. 4). We also identified a number of proteins involved in transcriptional activation and RNA-polymerase II-mediated transcription as PRDM5 interactors, including transcriptional activator protein Pur-alpha (PURA), NuRD-associated component TOP1 and FACT complex subunit proteins SPT16 and SSRP1 (Supplementary Material, Table S5).

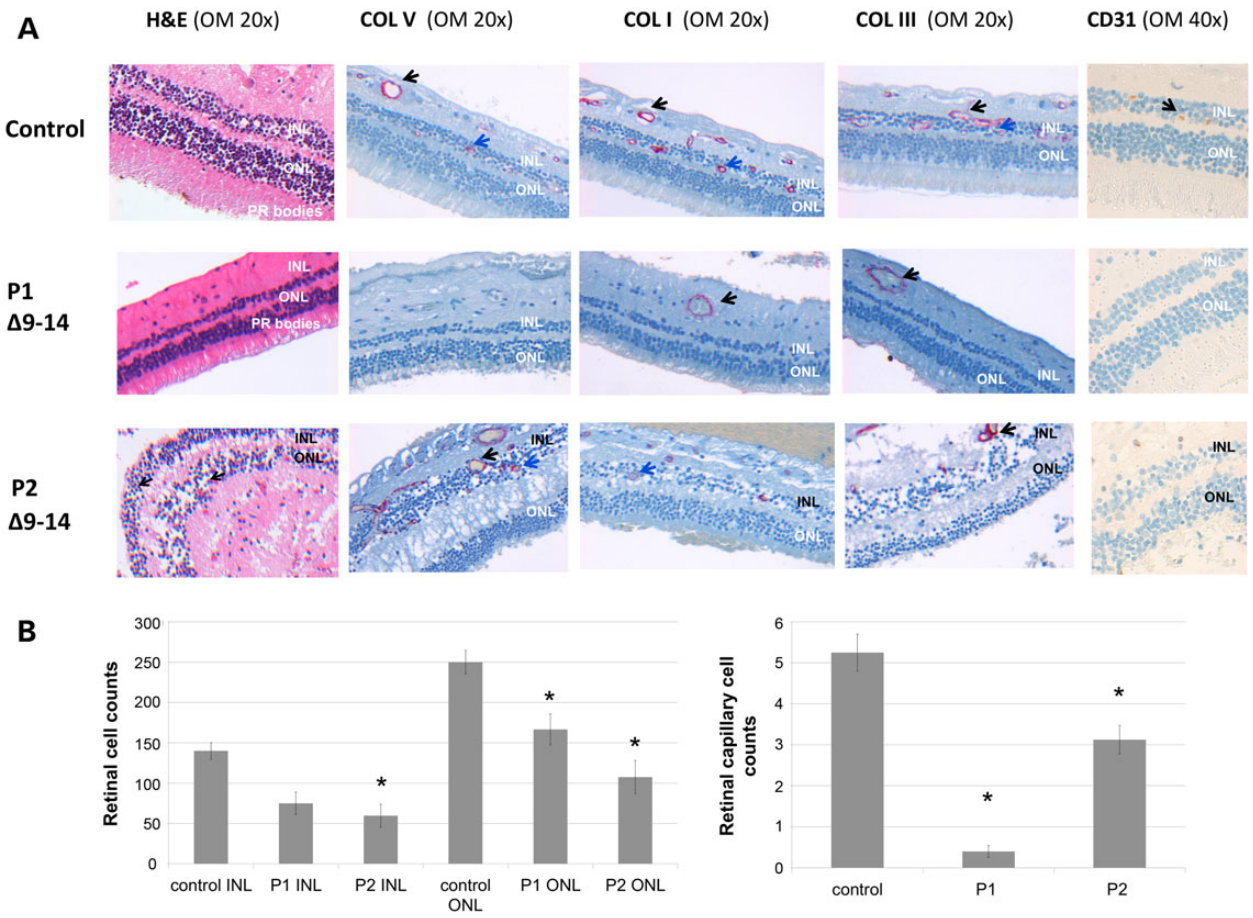

Figure 2. PRDM5-associated disease is associated with retinal thinning and abnormalities of retinal microvasculature in two individuals. (**A**) H&E stain and IHC for collagens V, I and III (red) and CD31 (brown) of unaffected control retina (#2—aged 58, Table 1) and BCS patients P1 and P2 carrying the *PRDM5* mutation Δexon9–14. H&E stain demonstrates diminished retinal cell densities in ONL and INL in P1 compared with the control [objective magnification (OM) 20×]. H&E staining of P2 retina shows retinal degenerative changes with disorganized anatomy of nuclei of the INL and ONL. IHC demonstrates a decrease in capillary staining (blue arrows) in BCS eyes P1 and P2 with decreased staining for collagens V, I and III and CD31 (middle and lower rows) versus a control sample (upper row). Staining for larger vessels such as retinal arterioles and venules persists (black arrow). Images were recorded and processed identically to allow direct comparisons to be made between them. (**B**) Graphical representations of retinal cell counts (left panel), and retinal capillary counts (right panel) in P1, P2 and control retina #2. Left panel: Mean retinal cell densities in the retinal INL and ONL confirming a significant (*) reduction in cell densities in the retinal INL in P2, and in both retinal INL and ONL in P1 ($P < 0.01$). Error bars represent 95% confidence intervals around the mean. Right panel: Reduction in retinal capillary staining for CD31 in both P1 and P2 BCS-type 2 retinas is statistically significant [$P < 0.01$ (*)].

A BCS-associated mutation diminishes the interaction of PRDM5 with repressive complexes

We then examined whether the BCS mutation p.Arg83Cys, present in patient P4, altered the PRDM5-interaction partners (Table 4). p.Arg83Cys is a deleterious mutation, predicted to interfere with binding of the ligand S-Adenosyl Methionine and its methylation reaction product, AdoHcy (Supplementary Material, Fig. S2). Thirteen proteins were identified as having significantly reduced or absent interaction with the mutant PRDM5 protein versus the WT control, using a fold change of average normalized spectral counts of ≥2 as a cut-off (Table 4). Proteins with reduced interaction were involved in chromatin modification (CHD4, TOP1), DNA transcriptional repression (HP1BP3, MYBBP1A), DNA transcriptional activation (PURA and SUPT16H) and translation and processing of mRNA (HNRNPR, LARP1, IGFBP2) (Table 2). A complete list of the proteins identified in the WT and mutant PRDM5 constructs are listed in Supplementary Material, Table S6. Normalized spectral counts (normalized to WT PRDM5 spectral counts) were used for interpretation. A further 34 proteins demonstrated unchanged or increased levels of interactions with the p.Arg83Cys mutant compared with the WT protein (Supplementary Material, Table S7).

Dysregulation of H3K9me2 in PRDM5-associated disease

The identification of HP1BP3 as a PRDM5 interactor (Table 2), and its loss when PRDM5 was mutated (Table 3 and Supplementary Material, Fig. S5), led us to investigate the expression of HP1BP3 *in vivo*, and investigate a possible role for repressive histone methylation marks, particularly H3K9 methylation, in the regulatory functions of PRDM5. We tested the expression of HP1BP3 in retinal tissue from two patients with the *PRDM5* Δexons 9–14 mutation (patients P1 and P2) using IHC, and found it was significantly decreased in BCS retinas compared with a control retina (#2, Table 1; $P < 0.01$) (Fig. 5A and B). Importantly, the reduction of HP1BP3 expression in BCS-affected tissue may be specific, as the expression of another PRDM5 interactor, SUPT16H (a FACT subunit protein with roles in transcriptional activation/RNA-polymerase 2 transcription) was unaltered between control and BCS-affected retinal tissue, suggesting that not all PRDM5

Table 2. Gene ontology analysis of dysregulated PRDM5-bound genes in skin fibroblasts of BCS2 patients

Gene ontology—Biological process	*P*-value	Adj *P*-value
(A)		
Blood vessel development	3.50E−05	2.10E−02
Vasculature development	4.00E−05	1.20E−02
Cell adhesion	5.30E−05	1.10E−02
Biological adhesion	5.40E−05	8.10E−03
Hemopoiesis	3.30E−04	3.90E−02
Cell morphogenesis involved in differentiation	3.80E−04	3.80E−02
Hemopoietic or lymphoid organ development	5.10E−04	4.40E−02
Immune system development	6.70E−04	5.00E−02
(B)		
Blood vessel development	2.10E−05	2.10E−02
Vasculature development	2.50E−05	1.30E−02
Blood vessel morphogenesis	6.60E−05	2.20E−02
Cell motion	8.20E−05	2.00E−02

Gene regulation status in expression MA data	Number of genes	Predicted PRDM5-binding ChIP-seq: UNBOUND	Predicted PRDM5-binding ChIP-seq: BOUND	% UNBOUND	Hypergeometric test *P*-value
(C)					
UP	178	135	43	24	0.029
Down	239	156	83	35	1.27E−09
Total	417	291	126	30	2.31E−09

Gene ontology analysis using DAVID for the most upregulated (A) and downregulated (B) genes in patient skin fibroblasts (from P2 and P3) versus control skin fibroblasts (107 and L10) in the expression microarray (Supplementary Material, Table S1) that were also found to be bound by PRDM5 in a ChIP-sequencing experiment (Supplementary Material, Table S2) (10) C. A hypergeometric test reveals that enrichment of dysregulated PRDM5-bound genes in patient skin fibroblasts is statistically significant. For each category (up or downregulated genes in our expression MA data (Supplementary Material, Table S1), we considered the number of genes that were PRDM5-bound or not (Supplementary Material, Table S2), out of the total number of genes that are up or down regulated in skin fibroblasts in each category. We then compared these results to the chance of finding a gene out of the ~20 000 in the genome bound by Prdm5 (out of a total of 3974 Prdm5-bound genes in the ChIP-seq data (10). Results indicate an enrichment of dysregulated PRDM5-bound genes in PRDM5-related disease.

interactors display reduced expression in BCS-affected tissue (data not shown).

We also examined the epigenetic modification H3K9me2 at upregulated (i.e. not repressed) ECM-related genes *COL13A1*, *NTN1* and *COL15A1* identified as direct PRDM5 transcriptional targets by ChIP-qPCR in control skin fibroblasts and found enrichment for H3K9me1/me2 at these genes (Fig. 3B). Expression of the H3K9me2 mark was also decreased in three patient cell lines (P1, P3, P5) compared with fibroblasts from unaffected age-matched controls (Fig. 6 and Supplementary Material, Fig. S6). Trimethylation marks H3K9me3 and H3K27me3 were not altered (data not shown).

Discussion

Our findings suggest that altered interactions of PRDM5 with repressive complexes, and altered epigenetic modifications surrounding the regulation of H3K9me2 play a role in PRDM5-associated disease. We suggest that the abnormal retinal vascular morphology seen in two related BCS2 patients with an in-frame deletion of exons 9–14 in *PRDM5* (Fig. 2) may result from a disruption in PRDM5 function in the transcription of ECM components concerned with vascular integrity and development. We identify epigenetic-related proteins as PRDM5-interaction partners (Fig. 4 and Tables 3 and 4); H3K9me2-mediated repression of ECM-related PRDM5-target genes with roles in vascular development and maintenance (Fig. 3B) and differential expression of both H3K9me2 in patient fibroblasts (Fig. 4) and HP1BP3 expression in retinal tissue (Fig. 5), versus controls. Our data suggest that altered expression of repressive complexes and H3K9me2 may be a feature of PRDM5-associated disease.

A strength of our study was the availability of human disease tissue samples to investigate the morphological effects of *PRDM5* mutations. The available samples were from a mixture of sources, but importantly came from patients with near-identical phenotypes. The Δexons 9–14 and p.Arg83Cys mutations are both predicted to significantly impair the function of PRDM5, providing an opportunity to analyse the impact of PRDM5 mutations on epigenetic modification. PRDM9 shares significant structural homology with PRDM5 in its PR domain and distal zinc finger structure (24), and the formation of the PRDM9—S-Adenosyl Methionine—AdoHcy histone substrate complex has been studied in detail (24). PRDM9 only folds in the presence of AdoHcy and H3K4me2, a major histone substrate of PRDM9 (24). Although PRDM5 may not have direct methyltransferase activity (7), the prediction that p.Arg83Cys (position equivalent to Tyr341 in PRDM9 (24), Supplementary Material, Fig. S2) impairs binding of S-Adenosyl Methionine and AdoHcy may still be relevant, particularly as this interaction is also predicted to be impaired by another BCS2 disease-causing mutation, p.Tyr107Cys.

Our work suggests that the retinal microvascular abnormalities and associated cellular loss seen in the retinas from patients

with type 2 BCS results from the dysregulation of ECM proteins due to the loss of PRDM5 function. Collagen 13 A1 has been associated with differentiation processes in vasculogenesis (26) and the C-terminal domains of collagen 15 A1, endostatin and restin, have potent anti-angiogenic activity (27–30). Netrin 1, an ECM glycoprotein, has been associated with both vascular development and pathological neovascularization (31), particularly in hypoxia (32–37). We confirmed H3K9me2 at upregulated (i.e. not repressed) ECM-related genes *COL13A1*, *NTN1* and *COL15A1* by ChIP-qPCR (Fig. 3B). Of note, none of the qPCR-confirmed downregulated genes [*COL4A2*, *BGN*, *PLOD2* (Supplementary Material, Fig. S4), and *COL4A1*, *COL11A1*, *HAPLN1*, *TGFβ2* (4)] demonstrated H3K9 methylation enrichment alongside PRDM5 binding in the ChIP-sequencing data.

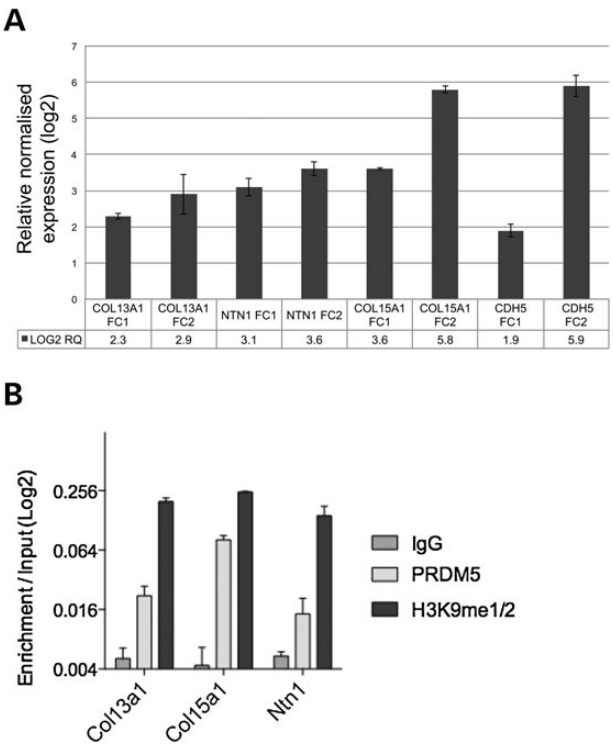

Figure 3. *PRDM5* mutations result in upregulation of a number of ECM-related genes with roles in vascular biology, with H3K9me2 being enriched in PRDM5-bound vasculogenesis-related genes. (**A**) qPCR analysis of BCS patient skin fibroblasts from P2 and P3 for PRDM5-target genes *COL13A1*, *NTN1*, *COL15A1* and *CDH5*. mRNA levels were normalized to *GAPDH*. The Y-axis represents fold changes in gene expression in logarithmic scale (log2). The X-axis shows the target assessed. FC1 = fold change in mRNA expression for skin fibroblasts of P2 and age-matched control fibroblasts 107 (Table 1). FC2 = fold change in mRNA expression for skin fibroblasts of P3 versus control fibroblasts L10 (Table 1). Error bars represent the 95% confidence intervals around the mean. Transcript levels of *COL13A1*, *NTN1*, *COL15A1* and *CDH5* were upregulated in BCS-type 2 mutant cell lines relative to controls with paired two-tailed t-test performed on the mean ΔCt values reaching statistical significance ($P < 0.01$) for all cell lines assessed. (**B**) ChIP-qPCR for PRDM5 and H3K9me1/2 at a subset of ECM-related genes with roles in vascular biology found to be upregulated in fibroblasts of P2, *PRDM5* Δ9–14; and P3, *PRDM5* p.Arg590* (Table 1). IgG is used as a negative control and values are indicated as % enrichment compared with input. Enrichment for H3K9 me1/2 is present at PRDM5-bound vasculogenesis-related genes *COL13A1*, *COL15A1* and *NTN1*.

PRDM5 interactors identified in pull-down experiments included major epigenetic modifiers, such as core components of the NuRD chromatin remodelling complex (38–40). NuRD proteins (e.g. MTA2 and CHD4, and associated component TOP1) interact with Prdm5 in embryonic stem cells (7) and have been implicated in developmental vasculogenesis (23). We also identified proteins associated with transcriptional activation, and RNA-polymerase II-mediated transcription as PRDM5-interacting proteins, including TOP1 (Supplementary Material, Table S5), believed to facilitate gene transcription by removing excess topological strain induced by the tracking of RNA polymerase. These findings are in keeping with the reported role of PRDM5 in RNA-polymerase II transcription regulation (10). However, as with all such studies, a degree of caution must be exercised when protein interactions are identified using exogenously expressed proteins in a cell line. Although this approach may not replicate the physiological situation, we did attempt to validate the salient observations in clinical samples whenever possible. We found a BCS2 p.Arg83Cys mutation in the PR domain of PRDM5 reduced its interaction with a number of proteins, including members of the NuRD co-repressor complex and other members of repressive complexes such as HP1BP3 and MYBBP1 (Table 4) and members of activator complexes including NuRD-associated component TOP1. The reduced interaction with CHD4 is noteworthy, as this NuRD complex ATPase regulates the transcription of ECM components around blood vessels during embryonic development in mice (23). H3K9 methylation also regulates the transcriptional activities of CHD4/NuRD, with H3K9 methylation bestowing additional affinity to CHD4/NuRD binding to nucleosomes, enhancing its repressive effect (41,42).

The p.Arg83Cys mutation also reduced the interaction with HP1BP3, a member of the repressive heterochromatin protein 1 (HP1) complex involved in chromatin organization (25,43) that binds H3K9 methylated genomic regions (25,44–45) (Table 4, Supplementary Material, Fig. S5). Interestingly, HP1 was previously reported as a Prdm5-interacting partner in mouse embryonic stem cells (7). We also observed decreased expression of HP1BP3 in the retinas of patients with the Δ exons 9–14 mutation in *PRDM5* (Fig. 5). These findings suggest a role for H3K9-interacting proteins in PRDM5 function.

Table 3. PRDM5 interactors identified by protein pull-down and mass spectrometry

Identified proteins (Human)	Gene name	Uniprot ID	MW (kDa)	Spectral counts						Average spectral counts	
				CTL1	CTL2	CTL3	WT1	WT2	WT3	Av CTL	Av WT
Chromodomain-helicase-DNA-binding protein 4	CHD4	Q14839	218	0	0	0	9	13	12	0	11
DNA topoisomerase 1	TOP1	P11387	91	0	0	0	18	9	6	0	11
Metastasis-associated protein MTA2	MTA2	O94776	75	0	0	0	5	10	10	0	8
Histone deacetylase 2	HDAC2	Q92769	66	2	0	0	7	8	7	1	7
Heterochromatin protein 1-binding protein 3	HP1BP3	Q9BQG0	61	0	0	0	7	6	5	0	6

Four proteins of the NuRD complex (CHD4, TOP1, MTA2 and HDAC2) were identified as significant PRDM5 interactors. Total and average spectral counts are shown. HP1BP3, a member of the heterochromatin protein 1 complex, was also identified.

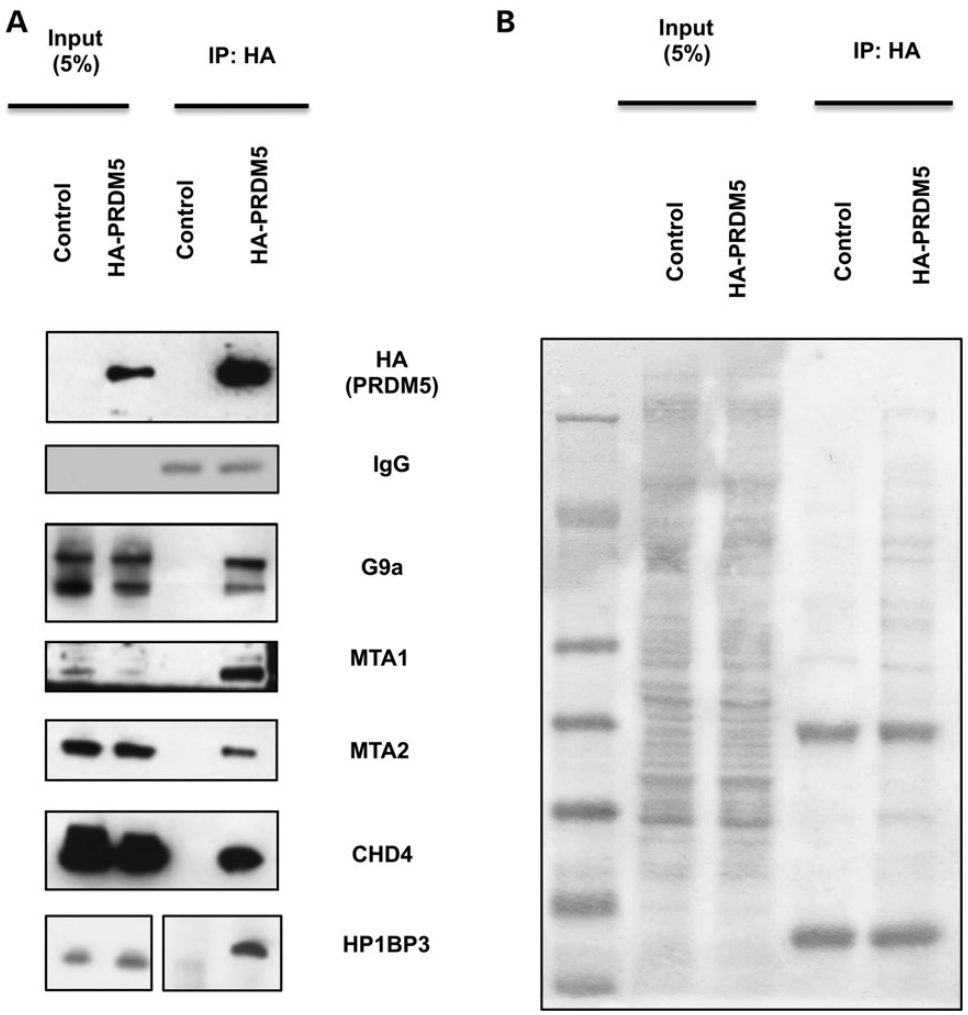

Figure 4. PRDM5 associates with NuRD complex components and HP1BP3. (**A**) Co-immunoprecipitation experiments between HA-tagged WT PRDM5 and specified endogenous HEK293 cell proteins for some NuRD complex proteins (MTA1, MTA2, CHD4) and HP1BP3. (**B**) Ponceau-S staining shows equal loading of protein samples.

How the expression of HP1BP3 is altered in the retina due to a mutation in PRDM5 is speculative. We investigated H3K9me2 expression in the adult retina of two healthy control patients (control #2 and control #1) and the retinas of two patients with BCS2 (P1 and P2) using IHC and were unable to detect H3K9me2 expression, despite strong staining in kidney and placental control tissues. These findings are in keeping with data from mouse retina that suggest H3K9me2 levels increase during retinal development (46–48), but that levels decline after retinogenesis, being virtually undetectable in adult mouse retina (48). Our results confirmed very low expression of H3K9me2 in adult human retinal tissue. It may be that the decreased H3K9 methylation levels established during retinogenesis in the presence of a PRDM5 mutation results in reduced HP1BP3 binding (46–48). This would contribute to the reduced HP1BP3 staining we observed in the retinas of two patients with PRDM5-associated disease. In this context, Katoh *et al.* (18) also speculated that decreased recruitment of H3K9me2-interacting proteins to the promoter of genes implicated in retinal survival might explain the retinal degenerative phenotype observed with conditional depletion of the H3K9 methyltransferase G9a in post-mitotic photoreceptor cells (18). It is also possible that HP1BP3, in the absence of its binding partner PRDM5, is less stable and thereby more easily degraded, as is the case for the PRC2 complex which is degraded when one of its protein components is inactivated (49).

Our observed dysregulation of an epigenetic regulatory mechanism in one of many inherited ocular diseases caused by a mutation in a transcription factor suggests that epigenetic modifications may be a more widespread disease mechanism in inherited eye disease. In other genetic conditions such as Kabuki Syndrome, mutations in two different epigenetic modifier genes *MLL2* (50) and *KDM6A* (51) acting on a common histone substrate have been described. MLL2 is a histone 3 lysine 4 (H3K4) N-methyltransferase and KDM6A is an H3K27 demethylase (50,51). In BCS, mutations in both *ZNF469* (BCS1) and *PRDM5* (BCS2) have been associated with the condition, with indistinguishable clinical phenotypes and the transcriptomes of patient fibroblasts with mutations in either *PRDM5* or *ZNF469* show considerable overlap (4,5). Both proteins have therefore been suggested to act in the same biological pathway although no direct protein–protein interaction has been demonstrated. It is possible that epigenetic regulatory mechanisms are relevant to both *ZNF469* and *PRDM5*-related BCS.

In conclusion, BCS type 2 has provided an opportunity to analyse the impact of mutations affecting PRDM5 on a repertoire of associated epigenetic modifiers, allowing us to propose a role

Table 4. Total spectrum count results from mass spectrometry identification of PRDM5-interaction partners showing proteins demonstrating reduced interaction with p.Arg83Cys PRDM5 mutant construct versus the WT

Identified proteins	Gene name	Uniprot ID	MW (kDa)	Spectral counts									Average raw spectral counts			Average normalized (to WT) spectral counts			Fold change
				CTL1	CTL2	CTL3	WT1	WT2	WT3	MUT1	MUT2	MUT3	Av CTL	Av WT	Av MUT	CTL	WT (+1)	MUT (+1)	WT/ MUT
La-related protein 1	LARP1	Q6PKG0	124	0	0	0	24	11	8	0	0	0	0	14	0	0	15	1	15
FACT complex subunit SPT16	*SUPT16H*	Q9Y5B9	120	0	0	0	14	12	13	0	0	0	0	13	0	0	14	1	14
DNA topoisomerase 1	*TOP1*	P11387	91	0	0	0	18	9	6	0	0	0	0	11	0	0	12	1	12
Insulin-like growth factor 2 mRNA-binding protein 2	IGF2BP2	P18065	67	0	0	0	12	6	11	0	0	0	0	10	0	0	11	1	11
Transcriptional activator protein Pur-alpha	*PURA*	Q00577	35	0	0	0	12	6	7	0	0	0	0	8	0	0	9	1	9
ATP-dependent RNA helicase DDX18	DDX18	Q9NVP1	75	0	0	0	11	5	7	0	0	0	0	8	0	0	9	1	9
F-box only protein 11	FBXO11	Q6X9E4	104	0	0	0	9	6	6	0	0	0	0	7	0	0	8	1	8
Heterochromatin protein 1-binding protein 3	HP1BP3	Q5S5J5	61	0	0	0	7	6	5	0	0	0	0	6	0	0	7	1	7
Small nuclear ribonucleoprotein Sm D2	SNRPD2	P62316	14	0	0	0	10	5	2	0	0	0	0	6	0	0	7	1	7
Splicing factor 3B subunit 1	SF3B1	O75533	146	0	0	0	5	10	4	0	0	0	0	6	0	0	7	1	7
Chromodomain-helicase-DNA-binding protein 4	CHD4	Q14839	218	0	0	0	9	13	12	0	0	3	0	11	1	0	12	5	2.4
Myb-binding protein 1A	MYBBP1A	Q9BQG0	149	0	0	0	18	17	7	4	0	0	0	14	1	0	15	7	2
Heterogeneous nuclear ribonucleoprotein R	HNRNPR	O43390	71	3	6	0	13	14	11	4	0	0	3	13	1	3	14	7	2

Normalized spectral counts (normalized to WT) and fold change of average normalized spectral counts of ≥2 are used. Highlighted in grey are the NuRD-associated proteins CHD4 and TOP1. HP1BP3 (in bold) also demonstrates reduced interaction with mutant PRDM5. Proteins involved in transcriptional activation and/or control of RNA-polymerase II-mediated transcription are shown in italics.

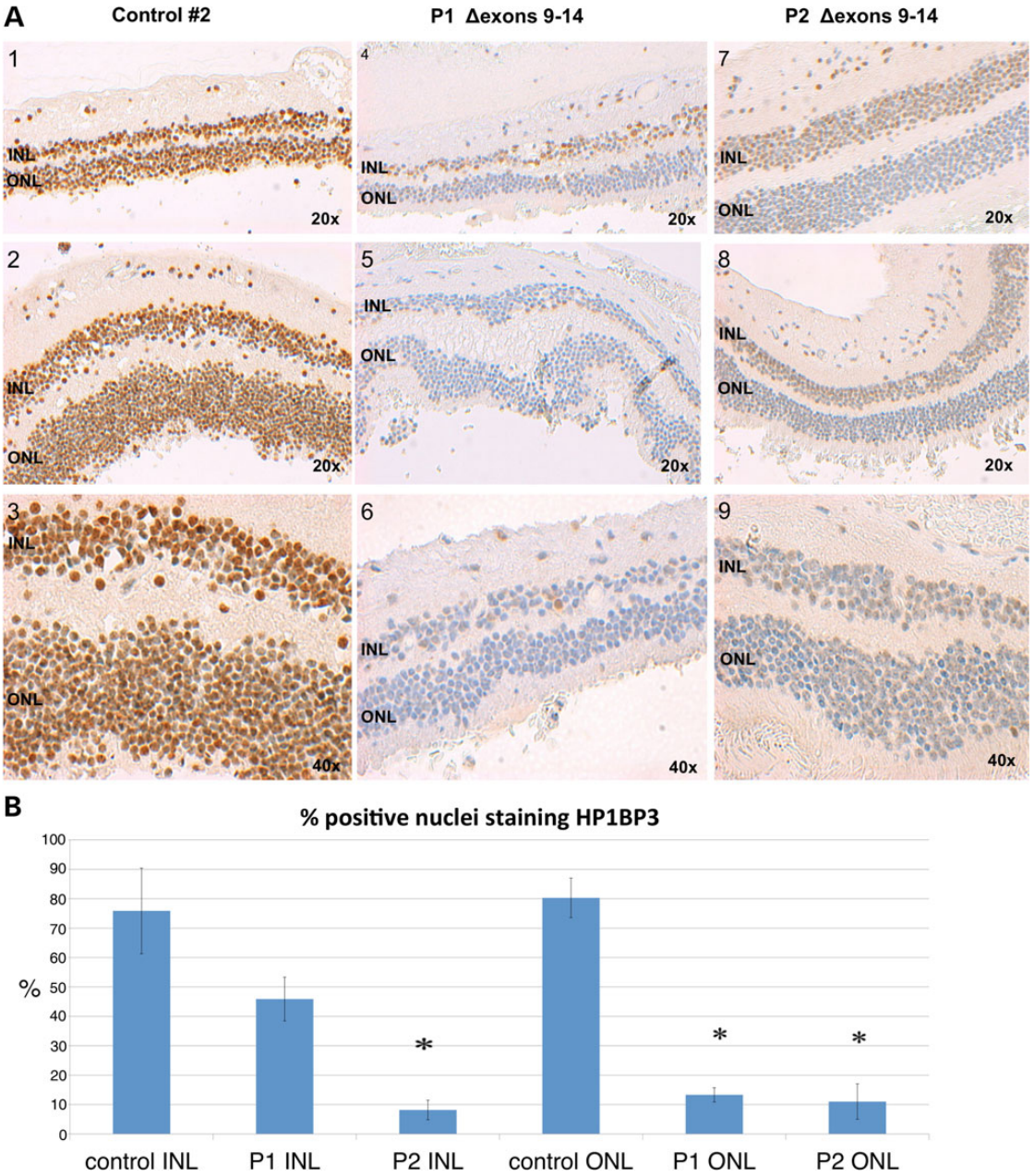

Figure 5. HP1BP3 expression is reduced in the retinas of two patients with BCS. Immunohistochemistry for HP1BP3. (**A**1 and 2). HP1BP3 staining in peripheral (1) and central retina (2) of a control eye (#2), showing nuclear staining for HP1BP3 in both the INL and ONL (OM 20×). (A3). HP1BP3 staining in control retina at higher magnification (OM 40×). (A4 and 5) HP1BP3 staining in peripheral (4) and central (5) retina of P2 with *PRDM5* Δexons9–14 (OM 20×), and P2 peripheral retina at higher magnification (OM 40×) (A6). (A7 and 8). HP1BP3 staining in peripheral (4) and central (5) retina of P1 with *PRDM5* Δexons9–14 (OM 20×), and P1 peripheral retina at higher magnification (OM 40×) (A9). Images were recorded and processed identically to allow direct comparisons to be made between them. (**B**) Graphical representation of percentage of HP1BP3-positive nuclei in INL and ONL for P1 and P2 versus a control sample (#2). Values are expressed as a mean of eight blinded cell counts. Error bars represent 95% confidence intervals around the mean. Results show a significant reduction in HP1BP3 staining (*) ($P < 0.01$) in the INL of P2 ($P = 0.006$), and a significant reduction in HP1BP3 staining for both P1 and P2 in the ONL ($P = 0.001$ for P1 and $P = 0.006$ for P2).

for defective interaction of repressive complexes and H3K9me2 in BCS type 2.

Materials and Methods

Subjects, clinical evaluation and genetic analyses

Informed written consent was obtained and investigations conducted in accordance with the principles of the Declaration of Helsinki, with Local Ethics Committee approval (NHS Research Ethics Committee reference 06/Q1406/52). Diagnosis of BCS in five patients [P1 and P2, with *PRDM5* Δ9–14; P3 with *PRDM5* p.Arg590*; P4 with *PRDM5* p.Arg83Cys, P5 with *PRDM5* p.Glu134* (Table 1)] was based on clinical examination and confirmed by mutation analysis of *ZNF469* (NM_001127464.1) and *PRDM5* (NM_018699.2), as described (3,4). A detailed ophthalmic, systemic, family and drug history was obtained. *PRDM5* variants identified in P4 were checked against control data sets including dbSNP

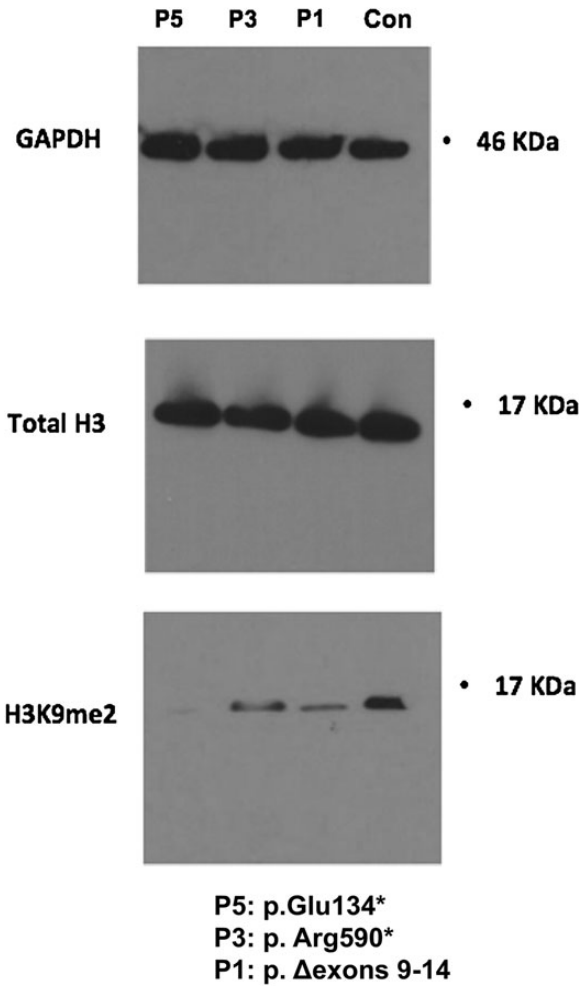

Figure 6. H3K9me2 is reduced in fibroblasts from patients with BCS2. Western blots of nuclear extracts of BCS patient fibroblasts with different *PRDM5* mutations and an unaffected control sample (4120) for: H3K9me2; GAPDH and total histone H3 (loading controls). P5; p.Glu134*; P3; p.Arg590*; P1; Δexons9–14; 4: control sample (4120, Table 1). Lanes were run on the same gel but were non-contiguous.

(Build 137) (http://www.ncbi.nlm.nih.gov/SNP), the 1000 Genomes Project (May 2012 release) (http://browser.1000genomes.org/index.html), and the NHLBI Exome Sequencing Project (http://evs.gs.washington.edu/EVS).

Clinical samples

A summary of the clinical samples used in this study is shown in Table 1. BCS-affected ocular tissue was obtained from the Department of Histopathology, Manchester Royal Infirmary. Human ocular tissue samples from control individuals were obtained from the Manchester Eye Bank (Table 1). Informed written consent and ethics committee approval was granted (14/NW/1495).

Computational modelling

We used the 3D-structure of the PRDM9 SET domain as a template (reference 24095733) to model the PRDM5 SET domain. These two domains share 30% sequence identity, which is sufficient to build a model that will give an overall impression of the domain. We used the WHAT IF (PMID: 2268628) & YASARA (PMID:11948792) Twinset for homology modelling and subsequent analysis.

Histology and immunohistochemistry

Histological analysis of BCS eyes was carried out in accordance with standard diagnostic protocols. 4 µm paraffin-embedded slides were stained with haematoxylin and eosin and elastin with van Gieson. Mouse monoclonal antibodies against collagen I (ab90395, Abcam); collagen III (ab6310, Abcam); collagen V (ab78056, Abcam); CD31 (clone JC70A, Dako); di-methyl histone 3 lysine 9 (H3K9me2) (Abcam ab1220) and rabbit polyclonal HP1BP3 (HPA 028215, Sigma-Aldrich), SUPT16H (Abcam ab204343) were used. Staining was performed on a Ventana Benchmark XT Automated Immunostaining Module (Ventana Medical Systems, Tucson, AZ, USA) together with the XT *ultra*-View Universal Red Alkaline Phosphatase detection system (Ventana Medical System) for all antibodies except H3K9me2, HP1BP3 and SUP16H, where DAB was used as the chromogen. Primary antibodies were diluted in Dako REAL™ Antibody Diluent (Dako, Agilent Technologies, UK) to the indicated optimal dilutions. The antibody dilutions were: collagen III, collagen V, CD31 and H3K9me2: 10 µg/ml; collagen I: 3 µg/ml; SUPT16H: 1 µg/ml and HP1BP3: 20 µg/ml, respectively. Collagen V antibody required heat-induced antigen retrieval using 0.2 M boric acid buffer pH7.0 at 60°C for 16 h. Sections of patient eye tissue were processed in parallel with the control tissue and were sorted and fixed in an identical manner. Tissue section slides were masked for origin and scored for cell densities in the retinal INL and ONL), the number of retinal capillaries and HP1BP3 nuclear staining, subjectively by an independent human observer. HP1BP3 nuclear staining was scored as present/absent and the tissue was considered positive when >20% of the cells displayed HP1BP3 nuclear staining. Eight blinded cell counts were performed for all observations with the means used to calculate statistical significance between patient and control samples using a non-parametric t-test with significance set at $P < 0.01$.

Chromatin immunoprecipitation

PRDM5 chromatin immunoprecipitation experiments and ChIP-seq data were previously published (10) and have been deposited in the NCBI GEO database (GSE62271, unlocked upon request). We re-analysed our previously published dataset by performing peak calling using MACS software (version 1.3.7.1), setting IgG signal for the background noise definition and a lower fold change cut-off for model building to 5. An additional significance cutoff was set to $P\text{-value} \leq 10^{-8}$. Gene annotation was performed using GREAT (52) and gene ontology of genes overlapping with microarray analysis was performed using DAVID (53).

Expression microarray analysis

Expression microarray was performed as previously described (4). The full data set was submitted to ArrayExpress (reference E-MEXP-3077). Transcripts with fold changes >3 compared with age and sex-matched controls in one of the two BCS cell lines studied, with a fold change ≥1.5 in the other BCS cell line in the same direction of effect were analysed with respect to PRDM5 binding using the ChIP-seq data described in the above section.

Quantitative PCR

Extracted total RNA was reverse-transcribed into single-stranded cDNA using a High Capacity RNA-to-cDNA Kit (Lifetechnologies,

Paisley, UK). RT-PCR was performed using first-strand cDNA with TaqMan Fast Universal PCR Master Mix (Life Technologies) as previously described (4). The assay numbers for the mRNA endogenous control (*GAPDH*) and target genes were as follows: *GAPDH* (Hs02758991_g1), *CDH5* (Hs00901464_m1), *COL13A1* (Hs00193225_m1), *NTN1* (Hs00924151_m1), *COL15A1* (Hs00266332_m1), *COL4A2* (Hs01098873_m1), *BGN* (Hs00959141_g), *PLOD2* (Hs01118190_m1) (Life Technologies).

ChIP-qPCR

Dermal fibroblasts growing in monolayer were crosslinked in 1% formaldehyde for 10 min at room temperature after which the reaction was stopped by addition of 0.125 M glycine. Cells were lysed and harvested in ChIP buffer (100 mM Tris at pH 8.6, 0.3% SDS, 1.7% Triton X-100 and 5 mM EDTA) and the chromatin disrupted by sonication using a Diagenode Bioruptor sonicator UCD-300 to obtain fragments of 200–500 bp in size. A total of 50 µg (measured as DNA) of chromatin was incubated with the following antibodies overnight: IgG (Sigma, I8140), Prdm5-Ab2 (7) and H3K9me1/2 (Abcam, Ab1220). Immunoprecipitated complexes were recovered on Protein-G dynabeads (Invitrogen) and, after extensive washes DNA was recovered by reverse crosslinking (incubation for 8 h at 65°C in 0.1 M Sodium Bicarbonate and 1% SDS in TE buffer) and purification using QIAquick PCR purification kit (Qiagen, Manchester, UK). qPCR was performed on a StepOne Plus system (Life Technologies) using Fast SYBR green reagents (Life Technologies) according to manufacturer's recommendations. Primers used for ChIP-qPCR included: ChIP_Col13a1_fwd, TGCCCTGAGAGTCACCTTTAGT; ChIP_Col13a1_rev, TGTCTTCAGAGGTTTGACCAGA; ChIP_Col15a1_fwd, GACACTGGTTTACCTGGCTTTC; ChIP_Col15a1_rev, CTGAAACGTTTAGCAAATTCCA; ChIP_Ntn1_fwd, CTGAAATCTGGAGAGGGATTTG; ChIP_Ntn1_rev, GCCTCTGAGTGTGTTTGTGAAG.

DNA constructs

Both Myc and HA-tagged PRDM5 in pcDNA3.1 have been described (6,7). Myc-*PRDM5* c.247c>t encoding the *PRDM5* p.Arg83Cys mutation was generated using the QuickChange II XL site-directed mutagenesis kit (Stratagene, CA, USA) using primers 5′-GCACTCCAACTGGCTTTGCTTCGTTCATGAGGC-3′ (forward sequence) and 5′-GCCTCATGAACGAAGCAAAGCCAGTTGCACTGC-3′ (reverse sequence).

HEK293 cell culture, transfection and extract preparation

HEK293 EBNA cells were grown and routinely maintained as above. Equal cell numbers were transfected using Effectene transfection reagent (Qiagen) according to the manufacturer's protocol. Extracts from HEK293 cells were harvested and lysed in RIPA buffer [containing 50 mM Tris (pH 8), 150 mM NaCl, 1% triton-X100, 0.5% deoxycholic acid, 0.1% SDS and protease and phosphatase inhibitors (Roche mini-Complete EDTA-free)]. Eluates were analysed by SDS-page on 4–12% bis-tris protein gels (LifeTechnologies) and expression confirmed by western blotting using anti c-myc antibody (anti-c myc monoclonal, Roche), HA (Biosite, PRB-101C) and GAPDH (Santa Cruz) (Supplementary Material, Fig. S7).

Immunoprecipitation and pull-down

Pull-down experiments were performed using lysates from HEK293 EBNA cells transiently expressing either WT or p.Arg83Cys myc-tagged or HA-tagged PRDM5. Untransfected HEK293 EBNA cells undergoing identical experimental steps in parallel were used as a control. *In vivo* crosslinking was performed. Co-immunoprecipitation experiments were performed using Myc and HA agarose beads (Sigma-Aldrich, Gillingham, UK). Antibodies used for co-immunoprecipitations were: HA (Biosite, PRB-101C), G9a (MBL bio D141-3), MTA1 (Abcam Ab751), MTA2 (Abcam, Ab8106), CHD4 (Santa Cruz, SC12541) and HP1BP3 (Sigma-Aldrich SAB1407417) as described previously (7). In brief, control untransfected HEK293 cells, WT HA-PRDM5 cells, WT myc-PRDM5 cells and mutant p.Arg83Cys myc-PRDM5 cells were crosslinked with 2.5 mM DSS for 30 min, before the reaction was quenched with 10–20 mM Tris, pH 7.5 final concentration. Cells were washed in PBS before being lysed in RIPA buffer. Lysates were incubated on ice for 30 min and cleared by centrifugation. The supernatant was removed and the clearing step repeated. Each complex (WT, p.Arg83Cys and control cells) was run in triplicate. Following a pre-clearing step using Sepharose protein G Fast-flow agarose (Sigma-Aldrich), lysates were incubated at 4°C with anti-myc agarose beads (Sigma-Aldrich) overnight. Myc-PRDM5 protein complexes were eluted from the beads with 20 µl 2× SDS sample buffer and incubated at 95 °C for 5 min. The eluates were run on a 10% NuPAGE gel (Lifetechnologies) and run at 200 V until the dye front was 1 cm into NuPAGE gel, enabling in-gel buffer exchange and total protein collection. Gels were washed in Milli-Q water (Merck Millipore) before staining with Instant Blue (Expedeon) for 1 h. Gels were de-stained by washing overnight in Milli-Q water.

Mass spectrometry analyses of PRDM5 complexes

The protein bands were excised from the gel and in-gel digestion performed as per Shevchenko *et al.* (54). Samples were analysed by LC-MS/MS using an UltiMate® 3000 Rapid Separation LC (RSLC, Dionex Corporation, Sunnyvale, CA, USA) coupled to an Orbitrap Elite (Thermo Fisher Scientific, Waltham, MA, USA) mass spectrometer. Peptide mixtures were separated using a gradient including 92% buffer A (0.1% formic acid in water) and 8% buffer B (0.1% FA in acetonitrile); to 33% buffer B (104 min at 300 nl min^{-1}); then 60% buffer B (105 min at 300 nl min^{-1}) using a 250 mm × 75 µm i.d. 1.7 mM BEH C18 analytical column (Waters). Peptides were selected for fragmentation automatically by data-dependent analysis.

Data processing and functional analyses of PRDM5 complexes

The acquired data were processed with the standard pipeline of Progenesis version 4.1 to obtain label-free quantification values, where peptides and proteins are identified using MASCOT (www.matrixscience.com) matching all MS-MS spectra against the human sequences from Uniprot May 2013 database. Carbamidomethylated cysteins were set as fixed and oxidation of methionine and N-terminal acetylation as variable modifications. The triplicates of each bait immunoprecipitation (IP) were analysed against the three control IPs. The following criteria were used to identify proteins and the following confidence filters selected to reduce peptide and protein global false discovery rate to <1: 99% protein confidence, 95% peptide confidence and minimum of three peptide identifications with at least two unique peptides. Significant interactors were determined by a volcano plot245-based strategy, combining *t*-test *P*-value and ratio information. *T*-test based comparison of bait IPs versus control IPs was performed with *P*-value threshold set at 0.05 and a bend of the curve value set at 1. Label-free quantification protein intensity

ratios of bait relative to control was plotted against the negative logarithmic *P*-value of the *t*-test as a stipulated line representing the permutation-based false discovery rate separating specific from non-specific binders. Data were also processed independently to generate total spectral count analyses with a protein confidence of 95%, by processing each sample dataset through Mascot version 2.4 for protein identification and Proteome-Software Scaffold version 4.0.8 (55) to qualify and validate those results. Three datasets were generated for each construct [control (CTL), wild-type (WT), mutant (MUT)]. Comparisons between peptides identified in the WT PRDM5 construct and control; as well as between WT PRDM5 construct and a BCS-mutant p.Arg83Cys PRDM5 construct were performed (Supplementary Material, Fig. S8).

To determine co-isolated proteins that were enriched in PRDM5 derivatives versus the control, the following spectral counting approach was performed (56): (1) spectral counts from biological replicates were averaged; (2) proteins with <5 average spectral counts in at least one condition were excluded; (3) proteins with ≥3-fold enrichment in PRDM5 WT isolation (versus control) were retained; (4) spectral counts for co-isolated proteins from the PRDM5 WT and PRDM5 p.Arg83Cys conditions were normalized by the factor 'PRDM5 WT spectral counts/PRDM5 mutant spectral counts' and finally (5) proteins with ≥3-fold enrichment in PRDM5 WT isolation (versus control) were retained for further gene ontology analysis using DAVID (53). Proteins with a cytoplasm cellular component gene ontology term, but lacking nuclear, nucleoplasm or nucleolus gene ontology terms were excluded. Upregulated peptides were detected by dividing the normalized peptide counts of the WT PRDM5 construct by the CTRL (WT/CTRL), or the WT PRDM5 construct by the mutant construct (WT/MUT), with a minimum of 2 fold difference and ≥to 5 peptides difference. Downregulated peptides were determined by analysis of normalized spectral counts of CTRL/WT and/or MUT/WT with a minimum of 2 fold difference and ≥5 peptides. A spectral count of 1 was added to all total spectral counts to facilitate calculation of fold enrichment of downregulated peptides.

Fibroblast cell culture and immunoblotting

Primary dermal fibroblast cultures were established from skin biopsies by routine procedures. Control samples were obtained from normal skin of age and sex-matched patients. Fibroblasts were maintained in DMEM supplemented with 10% fetal calf serum (PAA, Somerset, UK) at 37°C in 5% CO_2, expanded until confluent and harvested by trypsin treatment at the same passage number (between 6 and 9 passages). Fibroblast cell lysis and preparation of nuclear extracts were performed according to Schnitzler GR (57). Total protein content was quantified using a BioRad protein quantification BCA assay (BioRad Laboratories, Hemel Hempstead, UK). Skin fibroblasts nuclear extracts were subjected to standard SDS-PAGE using the following antibodies: di-methyl histone 3 lysine 9 (H3K9me2) (Abcam ab1220), tri-methyl histone 3 lysine 9 (H3K9me3) (Abcam ab8898); tri-methyl H3K27 (H3K27me3) (Abcam ab6002) and loading controls total H3 (Cell Signalling Technology, #9715) and GAPDH (Santa Cruz sc-47724). Experiments were performed on equal amounts of nuclear fraction protein (nuclear extracts 10μg). Membranes were blocked with TBST (0.1% Tween 20) containing 5% non-fat dry milk, and incubated with primary antibodies overnight. Visualization was performed with an enhanced chemiluminescence western blotting kit (Cell Signalling Technologies #7003).

Supplementary Material

Supplementary Material is available at *HMG* online.

Acknowledgements

We would like to thank Catherine Keeling and Martyna Kamieniorz for immunohistochemistry technical support, Dr Cecilia Giunta for patient recruitment, Professor Marshall Horwitz for the kind gift of the Myc-PRDM5 plasmid and the Manchester Eye Bank for the supply of control eye material.

Conflict of Interest statement. The authors declare that no conflict of interest exists.

Funding

L.F.P. is supported by a National Institute of Health Research (NIHR) pre-doctoral fellowship (NIHR-BRF-2011-015). G.C.B. and F.D.M. are partly supported by a grant from Action Medical Research (reference 1967). The project was supported by funding from NIHR Manchester Biomedical Research Centre. G.G.G. is supported by an American-Italian Cancer Foundation postdoctoral research fellowship.

References

1. Stein, R., Lazar, M. and Adam, A. (1968) Brittle cornea. A familial trait associated with blue sclera. *Am. J. Ophthalmol.*, **66**, 67–69.
2. Burkitt Wright, E.M., Porter, L.F., Spencer, H.L., Clayton-Smith, J., Au, L., Munier, F.L., Smithson, S., Suri, M., Rohrbach, M., Manson, F.D. *et al.* (2013) Brittle cornea syndrome: recognition, molecular diagnosis and management. *Orphanet J. Rare Dis.*, **8**, 68.
3. Abu, A., Frydman, M., Marek, D., Pras, E., Nir, U., Reznik-Wolf, H. and Pras, E. (2008) Deleterious mutations in the Zinc-Finger 469 gene cause brittle cornea syndrome. *Am. J. Hum. Genet.*, **82**, 1217–1222.
4. Burkitt Wright, E.M., Spencer, H.L., Daly, S.B., Manson, F.D., Zeef, L.A., Urquhart, J., Zoppi, N., Bonshek, R., Tosounidis, I., Mohan, M. *et al.* (2011) Mutations in PRDM5 in brittle cornea syndrome identify a pathway regulating extracellular matrix development and maintenance. *Am. J. Hum. Genet.*, **88**, 767–777.
5. Rohrbach, M., Spencer, H.L., Porter, L.F., Burkitt-Wright, E.M., Bürer, C., Janecke, A., Bakshi, M., Sillence, D., Al-Hussain, H., Baumgartner, M. *et al.* (2013) ZNF469 frequently mutated in the brittle cornea syndrome (BCS) is a single exon gene possibly regulating the expression of several extracellular matrix components. *Mol. Genet. Metab.*, **109**, 289–295.
6. Duan, Z., Person, R.E., Lee, H.H., Huang, S., Donadieu, J., Badolato, R., Grimes, H.L., Papayannopoulou, T. and Horwitz, M.S. (2007) Epigenetic regulation of protein-coding and microRNA genes by the Gfi1-interacting tumor suppressor PRDM5. *Mol. Cell Biol.*, **27**, 6889–6902.
7. Galli, G.G., Carrara, M., Francavilla, C., de Lichtenberg, K.H., Olsen, J.V., Calogero, R.A. and Lund, A.H. (2013) Genomic and proteomic analyses of Prdm5 reveal interactions with insulator binding proteins in embryonic stem cells. *Mol. Cell Biol.*, **33**, 4504–4516.
8. Huang, S., Shao, G. and Liu, L. (1998) The PR domain of the Rb-binding zinc finger protein RIZ1 is a protein binding interface

and is related to the SET domain functioning in chromatin-mediated gene expression. *J. Biol. Chem.*, **273**, 15933–15939.
9. Fog, C.K., Galli, G.G. and Lund, A.H. (2012) PRDM proteins: important players in differentiation and disease. *Bioessays*, **34**, 50–60.
10. Galli, G.G., Honnens de Lichtenberg, K., Carrara, M., Hans, W., Wuelling, M., Mentz, B., Multhaupt, H.A., Fog, C.K., Jensen, K. T., Rappsilber, J. *et al.* (2012) Prdm5 regulates collagen gene transcription by association with RNA polymerase II in developing bone. *PLoS Genet.*, **8**, e1002711.
11. Deng, Q. and Huang, S. (2004) PRDM5 is silenced in human cancers and has growth suppressive activities. *Oncogene*, **23**, 4903–4910.
12. Watanabe, Y., Toyota, M., Kondo, Y., Suzuki, H., Imai, T., Ohe-Toyota, M., Maruyama, R., Nojima, M., Sasaki, Y., Sekido, Y. *et al.* (2007) PRDM5 identified as a target of epigenetic silencing in colorectal and gastric cancer. *Clin. Cancer Res.*, **13**, 4786–4794.
13. Cheng, H.Y., Chen, X.W., Cheng, L., Liu, Y.D. and Lou, G. (2010) DNA methylation and carcinogenesis of PRDM5 in cervical cancer. *J. Cancer Res. Clin. Oncol.*, **136**, 1821–1825.
14. Shu, X.S., Geng, H., Li, L., Ying, J., Ma, C., Wang, Y., Poon, F.F., Wang, X., Ying, Y., Yeo, W. *et al.* (2011) The epigenetic modifier PRDM5 functions as a tumor suppressor through modulating WNT/beta-catenin signaling and is frequently silenced in multiple tumors. *PLoS One*, **6**, e27346.
15. Galli, G.G., Multhaupt, H.A., Carrara, M., de Lichtenberg, K.H., Christensen, I.B., Linnemann, D., Santoni-Rugiu, E., Calogero, R.A. and Lund, A.H. (2014) Prdm5 suppresses Apc-driven intestinal adenomas and regulates monoacylglycerol lipase expression. *Oncogene*, **33**, 3342–3350.
16. Tan, S.X., Hu, R.C., Tan, Y.L., Liu, J.J. and Liu, W.E. (2014) Promoter methylation-mediated downregulation of PRDM5 contributes to the development of lung squamous cell carcinoma. *Tumour Biol.*, **35**, 4509–4516.
17. Rao, R.C., Tchedre, K.T., Malik, M.T., Coleman, N., Fang, Y., Marquez, V.E. and Chen, D.F. (2010) Dynamic patterns of histone lysine methylation in the developing retina. *Invest. Ophthalmol. Vis. Sci.*, **51**, 6784–6792.
18. Katoh, K., Yamazaki, R., Onishi, A., Sanuki, R. and Furukawa, T. (2012) G9a histone methyltransferase activity in retinal progenitors is essential for proper differentiation and survival of mouse retinal cells. *J. Neurosci.*, **32**, 17658–17670.
19. Tachibana, M., Ueda, J., Fukuda, M., Takeda, N., Ohta, T., Iwanari, H., Sakihama, T., Kodama, T., Hamakubo, T. and Shinkai, Y. (2005) Histone methyltransferases G9a and GLP form heteromeric complexes and are both crucial for methylation of euchromatin at H3-K9. *Genes Dev.*, **19**, 815–826.
20. Tachibana, M., Matsumura, Y., Fukuda, M., Kimura, H. and Shinkai, Y. (2008) G9a/GLP complexes independently mediate H3K9 and DNA methylation to silence transcription. *EMBO J.*, **27**, 2681–2690.
21. Rai, K., Jafri, I.F., Chidester, S., James, S.R., Karpf, A.R., Cairns, B.R. and Jones, D.A. (2010) Dnmt3 and G9a cooperate for tissue-specific development in zebrafish. *J. Biol. Chem.*, **285**, 4110–4121.
22. Ingram, K.G., Curtis, C.D., Silasi-Mansat, R., Lupu, F. and Griffin, C.T. (2013) The NuRD chromatin-remodeling enzyme CHD4 promotes embryonic vascular integrity by transcriptionally regulating extracellular matrix proteolysis. *PLoS Genet.*, **9**, e1004031.
23. Wu, H., Mathioudakis, N., Diagouraga, B., Dong, A., Dombrovski, L., Baudat, F., Cusack, S., de Massy, B. and Kadlec, J. (2013) Molecular basis for the regulation of the H3K4 methyltransferase activity of PRDM9. *Cell Rep.*, **5**, 13–20.
24. Hayashihara, K., Uchiyama, S., Shimamoto, S., Kobayashi, S., Tomschik, M., Wakamatsu, H., No, D., Sugahara, H., Hori, N., Noda, M. *et al.* (2010) The middle region of an HP1-binding protein, HP1-BP74, associates with linker DNA at the entry/exit site of nucleosomal DNA. *J. Biol. Chem.*, **285**, 6498–6507.
25. Heikkinen, A., Tu, H. and Pihlajaniemi, T. (2012) Collagen XIII: a type II transmembrane protein with relevance to musculoskeletal tissues, microvessels and inflammation. *Int. J. Biochem. Cell. Biol.*, **44**, 714–717.
26. Ramchandran, R., Dhanabal, M., Volk, R., Waterman, M.J., Segal, M., Lu, H., Knebelmann, B. and Sukhatme, V.P. (1999) Antiangiogenic activity of restin, NC10 domain of human collagen XV: comparison to endostatin. *Biochem. Biophys. Res. Commun.*, **255**, 735–739.
27. Tomono, Y., Naito, I., Ando, K., Yonezawa, T., Sado, Y., Hirakawa, S., Arata, J., Okigaki, T. and Ninomiya, Y. (2002) Epitope-defined monoclonal antibodies against multiplexin collagens demonstrate that type XV and XVIII collagens are expressed in specialized basement membranes. *Cell Struct. Funct.*, **27**, 9–20.
28. Marneros, A.G. and Olsen, B.R. (2001) The role of collagen-derived proteolytic fragments in angiogenesis. *Matrix Biol.*, **20**, 337–345.
29. Sasaki, T., Larsson, H., Tisi, D., Claesson-Welsh, L., Hohenester, E. and Timpl, R. (2000) Endostatins derived from collagens XV and XVIII differ in structural and binding properties, tissue distribution and anti-angiogenic activity. *J Mol. Biol.*, **301**, 1179–1190.
30. Wilson, B.D., Ii, M., Park, K.W., Suli, A., Sorensen, L.K., Larrieu-Lahargue, F., Urness, L.D., Suh, W., Asai, J., Kock, G.A. *et al.* (2006) Netrins promote developmental and therapeutic angiogenesis. *Science*, **313**, 640–644.
31. Tian, X.F., Xia, X.B., Xiong, S.Q., Jiang, J., Liu, D. and Liu, J.L. (2011) Netrin-1 overexpression in oxygen-induced retinopathy correlates with breakdown of the blood-retina barrier and retinal neovascularization. *Ophthalmologica*, **226**, 37–44.
32. Ramkhelawon, B., Yang, Y., van Gils, J.M., Hewing, B., Rayner, K.J., Parathath, S., Guo, L., Oldebeken, S., Feig, J.L., Fisher, E.A. *et al.* (2013) Hypoxia induces netrin-1 and Unc5b in atherosclerotic plaques: mechanism for macrophage retention and survival. *Arterioscler. Thromb. Vasc. Biol.*, **33**, 1180–1188.
33. Cayre, M., Courtès, S., Martineau, F., Giordano, M., Arnaud, K., Zamaron, A. and Durbec, P. (2013) Netrin 1 contributes to vascular remodeling in the subventricular zone and promotes progenitor emigration after demyelination. *Development*, **140**, 3107–3117.
34. He, X., Li, Y., Lu, H., Zhang, Z., Wang, Y. and Yang, G.Y. (2013) Netrin-1 overexpression promotes white matter repairing and remodeling after focal cerebral ischemia in mice. *J. Cereb. Blood Flow Metab.*, **33**, 1921–1927.
35. Lu, H., Wang, Y., He, X., Yuan, F., Lin, X., Xie, B., Tang, G., Huang, J., Tang, Y., Jin, K. *et al.* (2012) Netrin-1 hyperexpression in mouse brain promotes angiogenesis and long-term neurological recovery after transient focal ischemia. *Stroke*, **43**, 838–843.
36. Sherpa, T., Lankford, T., McGinn, T.E., Hunter, S.S., Frey, R.A., Sun, C., Ryan, M., Robison, B.D. and Stenkamp, D.L. (2014) Retinal regeneration is facilitated by the presence of surviving neurons. *Dev. Neurobiol.*, **74**, 851–876.
37. Xue, Y., Wong, J., Moreno, G.T., Young, M.K., Cote, J. and Wang, W. (1998) NURD, a novel complex with both

ATP-dependent chromatin-remodeling and histone deacetylase activities. *Mol. Cell*, **2**, 851–861.
38. Allen, H.F., Wade, P.A. and Kutateladze, T.G. (2013) The NuRD architecture. *Cell Mol. Life Sci.*, **70**, 3513–3524.
39. Ramirez, J. and Hagman, J. (2009) The Mi-2/NuRD complex: a critical epigenetic regulator of hematopoietic development, differentiation and cancer. *Epigenetics*, **4**, 532–536.
40. Musselman, C.A., Mansfield, R.E., Garske, A.L., Davrazou, F., Kwan, A.H., Oliver, S.S., O'Leary, H., Denu, J.M., Mackay, J.P. and Kutateladze, T.G. (2009) Binding of the CHD4 PHD2 finger to histone H3 is modulated by covalent modifications. *Biochem. J.*, **423**, 179–187.
41. Musselman, C.A., Ramírez, J., Sims, J.K., Mansfield, R.E., Oliver, S.S., Denu, J.M., Mackay, J.P., Wade, P.A., Hagman, J. and Kutateladze, T.G. (2012) Bivalent recognition of nucleosomes by the tandem PHD fingers of the CHD4 ATPase is required for CHD4-mediated repression. *Proc. Natl. Acad. Sci. USA*, **109**, 787–792.
42. Dutta, B., Ren, Y., Hao, P., Sim, K.H., Cheow, E., Adav, S., Tam, J. P. and Sze, S.K. (2014) Profiling of the chromatin-associated proteome identifies HP1BP3 as a novel regulator of cell cycle progression. *Mol. Cell Proteomics.*, **13**, 2183–2197.
43. Lachner, M., O'Carroll, D., Rea, S., Mechtler, K. and Jenuwein, T. (2001) Methylation of histone H3 lysine 9 creates a binding site for HP1 proteins. *Nature*, **410**, 116–120.
44. Bannister, A.J., Zegerman, P., Partridge, J.F., Miska, E.A., Thomas, J.O., Allshire, R.C. and Kouzarides, T. (2001) Selective recognition of methylated lysine 9 on histone H3 by the HP1 chromo domain. *Nature*, **410**, 120–124.
45. Lechner, M.S., Schultz, D.C., Negorev, D., Maul, G.G. and Rauscher, F.J. (2005) The mammalian heterochromatin protein 1 binds diverse nuclear proteins through a common motif that targets the chromoshadow domain. *Biochem. Biophys. Res. Commun.*, **331**, 929–937.
46. Wen, B., Wu, H., Shinkai, Y., Irizarry, R.A. and Feinberg, A.P. (2009) Large histone H3 lysine 9 dimethylated chromatin blocks distinguish differentiated from embryonic stem cells. *Nat. Genet.*, **41**, 246–250.
47. Peric-Hupkes, D., Meuleman, W., Pagie, L., Bruggeman, S.W., Solovei, I., Brugman, W., Gräf, S., Flicek, P., Kerkhoven, R.M., van Lohuizen, M., Reinders, M. *et al.* (2010) Molecular maps of the reorganization of genome-nuclear lamina interactions during differentiation. *Mol. Cell*, **38**, 603–613.
48. Rao, R.C., Tchedre, K.T., Malik, M.T., Coleman, N., Fang, Y., Marquez, V.E. and Chen, D.F. (2010) Dynamic patterns of histone lysine methylation in the developing retina. *Invest. Ophthalmol. Vis. Sci.*, **51**, 6784–6792.
49. Pasini, D., Bracken, A.P., Jensen, M.R., Lazzerini Denchi, E. and Helin, K. (2004) Suz12 is essential for mouse development and for EZH2 histone methyltransferase activity. *EMBO J.*, **23**, 4061–4071.
50. Ng, S.B., Bigham, A.W., Buckingham, K.J., Hannibal, M.C., McMillin, M.J., Gildersleeve, H.I., Beck, A.E., Tabor, H.K., Cooper, G.M., Mefford, H.C. *et al.* (2010) Exome sequencing identifies MLL2 mutations as a cause of Kabuki syndrome. *Nat. Genet.*, **42**, 790–793.
51. Lederer, D., Grisart, B., Digilio, M.C., Benoit, V., Crespin, M., Ghariani, S.C., Maystadt, I., Dallapiccola, B. and Verellen-Dumoulin, C. (2012) Deletion of KDM6A, a histone demethylase interacting with MLL2, in three patients with Kabuki syndrome. *Am. J. Hum. Genet.*, **90**, 119–124.
52. McLean, C.Y., Bristor, D., Hiller, M., Clarke, S.L., Schaar, B.T., Lowe, C.B., Wenger, A.M. and Bejerano, G. (2010) GREAT improves functional interpretation of cis-regulatory regions. *Nat. Biotechnol.*, **28**, 495–501.
53. Huang da, W., Sherman, B.T. and Lempicki, R.A. (2009) Systematic and integrative analysis of large gene lists using DAVID bioinformatics resources. *Nat. Protoc.*, **4**, 44–57.
54. Shevchenko, A., Wilm, M., Vorm, O. and Mann, M. (1996) Mass spectrometric sequencing of proteins from silver stained polyacrylamide gels. *Anal. Chem.*, **68**, 850–858.
55. Searle, B.C. (2010) Scaffold: a bioinformatic tool for validating MS/MS-based proteomic studies. *Proteomics*, **10**, 1265–1269.
56. Florens, L. and Washburn, M.P. (2006) Proteomic analysis by multidimensional protein identification technology. *Methods Mol. Biol.*, **328**, 159–175.
57. Schnitzler, G.R. (2000) Isolation of histones and nucleosome cores from mammalian cells. In Ausubel, F.M., Brent, R., Kingston, R.E., Moore, D.D., Seidman, J.G., Smith, J.A. and Struhl, K. (eds), *Current Protocols in Molecular Biology*. Green Publishing/Wiley Interscience, New York, NY, USA, pp. 21.5.3–21.5.5.